JAMES | Journal of Advances in Modeling Earth Systems

RESEARCH ARTICLE
10.1029/2018MS001592

Cloud-Radiative Impact on the Regional Responses of the Midlatitude Jet Streams and Storm Tracks to Global Warming

Nicole Albern[1], **Aiko Voigt**[1,2], **and Joaquim G. Pinto**[1]

[1]Institute of Meteorology and Climate Research - Department Troposphere Research, Karlsruhe Institute of Technology, Karlsruhe, Germany, [2]Lamont-Doherty Earth Observatory, Columbia University, New York, NY, USA

Key Points:
- We investigate global atmosphere model simulations in present-day setup with prescribed SST and the cloud-locking method
- Cloud-radiative impact on jet response is substantial, and largely independent of season and SST pattern, but depends on the ocean basin
- Cloud-radiative impact is zonally symmetric, consistent with a zonally symmetric change in cloud-radiative heating in the midlatitudes

Supporting Information:
- Supporting Information S1

Correspondence to:
N. Albern,
nicole.albern@kit.edu

Citation:
Albern, N., Voigt, A., & Pinto, J. G. (2019). Cloud-radiative impact on the regional responses of the midlatitude jet streams and storm tracks to global warming. *Journal of Advances in Modeling Earth Systems*, *11*, 1940–1958. https://doi.org/10.1029/2018MS001592

Received 12 DEC 2018
Accepted 9 MAY 2019
Accepted article online 24 MAY 2019
Published online 2 JUL 2019

Abstract Previous work demonstrated the strong radiative coupling between clouds and the midlatitude circulation. Here we investigate the impact of cloud-radiative changes on the global warming response of the midlatitude jet streams and storm tracks in the North Atlantic, North Pacific, and Southern Hemisphere. To this end, we use the ICOsahedral Nonhydrostatic global atmosphere model in present-day setup and with the cloud-locking method. Sea surface temperatures are prescribed to isolate the circulation response to atmospheric cloud-radiative heating. In the annual mean, cloud-radiative changes contribute one to two thirds to the poleward jet shift in all three ocean basins and support the jet strengthening in the North Atlantic and Southern Hemisphere. Cloud-radiative changes also impact the storm track, but the impact is more diverse across the three ocean basins. The cloud-radiative impact on the North Atlantic and North Pacific jets varies little from season to season in absolute terms, whereas its relative importance changes over the course of the year. In the Southern Hemisphere, cloud-radiative changes strengthen the jet in all seasons, whereas their impact on the jet shift is limited to austral summer and fall. The cloud-radiative impact is largely zonally symmetric and independent of whether global warming is mimicked by a uniform 4 K or spatially varying sea surface temperatures increase. Our results emphasize the importance of cloud-radiative changes for the response of the midlatitude circulation to global warming, indicating that clouds can contribute to uncertainty in model projections of future circulations.

1. Introduction

The midlatitude jet streams and storm tracks dominate the heat, momentum, and moisture transport outside of the tropics (Chang et al., 2002; Hoskins & Valdes, 1990; Shaw et al., 2016). They are important components of the large-scale atmospheric circulation, because of which understanding their responses to global warming is essential for reliable predictions of regional climate change (e.g., Ulbrich et al., 2009). Jet streams and storm tracks, and their responses to global warming, were studied extensively during the last decades (e.g., Barnes & Polvani, 2013; Chang et al., 2012; Kushner et al., 2001; Simpson et al., 2014; Yin, 2005). Nevertheless, climate model projections of future changes in jets and storm tracks exhibit large uncertainties (Shepherd, 2014), and the factors controlling the location, strength, and variability of jet streams and storm tracks remain not fully understood (Bony et al., 2015; Shaw et al., 2016; Vallis et al., 2015). Here we focus on the coupling of clouds with the midlatitude circulation and study the role of cloud-radiative changes for the global warming response of the jet streams and storm tracks.

Global climate models suggest that the jet streams and storm tracks shift poleward in both hemispheres and that the Southern Hemisphere jet streams and storm tracks strengthen in response to global warming (e.g., Barnes & Polvani, 2013; Chang et al., 2012; Pinto et al., 2006; Simpson et al., 2014; Vallis et al., 2015; Yin, 2005). The response of the midlatitude circulation is related to changes in meridional temperature gradients and baroclinicity. As such, previous work studied the role of increased upper-tropospheric and decreased lower-tropospheric temperature gradients (e.g., Butler et al., 2010; Harvey et al., 2015; Lorenz & DeWeaver, 2007; Yin, 2005). These temperature changes can result from a multitude of factors, including moist convection (Vallis et al., 2015), ozone depletion (Polvani et al., 2011), and sea-ice loss (Vavrus, 2018; Zappa et al., 2018).

An additional factor that strongly projects on meridional temperature gradients is clouds and their radiative interactions. Cloud-radiative interactions were found to set the latitude of the Southern Hemisphere

jet stream (Ceppi et al., 2012) and strengthen the jet streams in present-day climate (Li et al., 2015). The poleward shifts of the Southern Hemisphere storm track and eddy-driven jet stream in global warming simulations were found to depend on the radiative response of Southern Ocean clouds (Ceppi et al., 2014; Ceppi & Shepherd, 2017; Grise & Polvani, 2014a). Li et al. (2019) found that atmospheric cloud-radiative effects enhance the poleward jet shift in response to global warming in present-day simulations that apply the Clouds On-Off Klimate Intercomparison Experiment framework (COOKIE; Stevens et al., 2012). Idealized global warming simulations in aquaplanet setups revealed that half or more of the poleward jet stream shift can be attributed to cloud-radiative changes (Ceppi & Hartmann, 2016; Voigt & Shaw, 2015). The aquaplanet work of Voigt and Shaw (2015, 2016) identified that cloud-radiative changes are important even when sea surface temperatures (SST) are prescribed, showing that a large part of the cloud-radiative impact results from the direct atmospheric cloud-radiative heating. This is supported by the study of Voigt et al. (2019), which investigated the cloud-radiative impact on the annual-mean zonal-mean jet stream response in a present-day setup. The authors decomposed the cloud-radiative impact into a surface and an atmospheric pathway, depending on whether SST are interactive or prescribed. They found that the atmospheric pathway of the cloud-radiative impact, that is, the impact of changes in atmospheric cloud-radiative heating in the absence of SST changes, is at least as important as the surface pathway, that is, the response of the surface temperature to surface cloud-radiative heating.

Given the importance of continents for shaping the midlatitude circulation (Brayshaw et al., 2009), we extend the aquaplanet studies and investigate the impact of cloud-radiative changes on the global warming response of the midlatitude jet streams and storm tracks in more realistic simulations that include present-day boundary conditions, that is, continents, sea ice, and a seasonal cycle. These simulations further allow us to study the cloud-radiative impact across seasons and ocean basins. This is important as the midlatitude circulation response varies substantially over the course of the year and across regions (Simpson et al., 2014; Zappa et al., 2015).

We investigate the impact of cloud-radiative changes on the annual-mean and seasonal-mean responses of the midlatitude jet streams and storm tracks to global warming in the North Atlantic, North Pacific, and Southern Hemisphere ocean. For this purpose, we perform simulations with the ICOsahedral Nonhydrostatic model (ICON; Zängl et al., 2015) and estimate the role of cloud-radiative changes with the cloud-locking method (e.g., Ceppi & Hartmann, 2016; Voigt & Shaw, 2015, 2016). SST are prescribed to isolate the impact of cloud-radiative changes when clouds do not affect SST, complementing the work of Ceppi and Shepherd (2017) with interactive SST. We compare two sets of global warming simulations that use different SST changes to mimic global warming. This allows us to study to what extent the cloud-radiative impact depends on the pattern of the surface warming, which Woollings et al. (2012) identified to shape the storm track response in the North Atlantic and over Europe.

We address the following questions:

1. How important is the cloud-radiative impact for the midlatitude jet stream and storm track responses to global warming in the North Atlantic, North Pacific, and Southern Hemisphere ocean?
2. To what extent does the cloud-radiative impact vary across seasons and ocean basins?
3. Does the cloud-radiative impact depend on the pattern of the SST increase?

The structure of the paper is as follows: Section 2 presents the model setup, the metrics for the midlatitude jet streams and storm tracks, and the application of the cloud-locking method to diagnose the impact of cloud-radiative changes. The annual-mean responses are discussed in section 3; the seasonal-mean responses are covered in section 4. In section 5, we show correlations between the jet stream and atmospheric temperature gradients. The main results are summarized and discussed in section 6.

2. Model Setup, Circulation Metrics, and Cloud-Locking Method

2.1. Model Setup and Midlatitude Circulation Metrics

We perform numerical simulations with the atmospheric component of ICON (Zängl et al., 2015). The model is run with the physics package used for numerical weather prediction (version 2.1.00). The simulations are performed in R2B04 horizontal resolution (approximately 160 km) with 47 levels extending up to 75 km. A time step of 720 s is used.

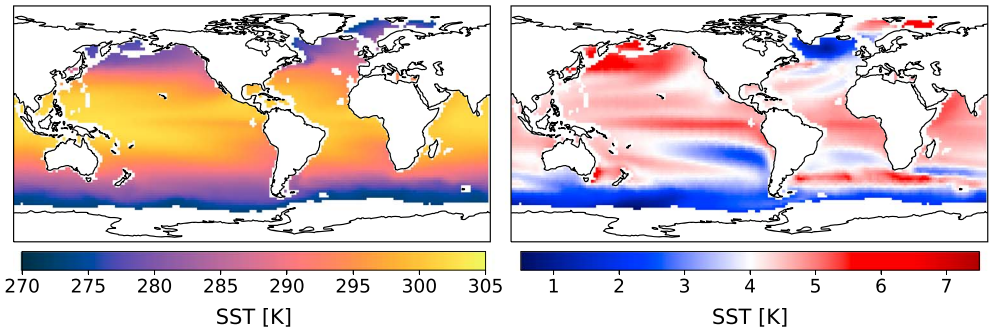

Figure 1. Annual-mean sea surface temperature (SST) pattern of the CTL simulation (left) and anomalous SST pattern used for the PAT simulation (right). Regions covered by land or more than 15% of sea ice are masked.

We use a present-day model setup with prescribed SST. SST are prescribed to isolate atmospheric cloud-radiative interactions, which primarily arise from longwave radiation (Allan, 2011). We use climatological SST and sea-ice fields, which are obtained by calculating multiyear monthly means of the SST and sea-ice fields over the Atmospheric Model Intercomparison Project (AMIP) period (1979–2008; Gates, 1992). The multiyear monthly means are prescribed to the model in the control simulation ("CTL"). The annual-mean SST pattern of the control simulation is shown in Figure 1 (left panel). In addition, we perform two sets of global warming simulations. In the first set, global warming is mimicked by a uniform 4 K SST increase ("UNI"), similar to the Amip4 K simulations that are part of the Coupled Model Intercomparison Project Phase 5 (CMIP5; Taylor et al., 2012). In the second set, global warming is mimicked by increasing the SST by a pattern ("PAT"), similar to the AmipFuture simulations in CMIP5. We use the same SST pattern that is used for the AmipFuture simulations and which is provided by Cloud Feedback Model Intercomparison Project (https://www.earthsystemcog.org/projects/cfmip/cfmip2-cmip5). The SST pattern is derived from the multimodel mean SST response simulated by CMIP3 global atmosphere-ocean models at the time of CO_2 quadrupling in the 1% CO_2 increase per year experiment (Taylor et al., 2009, 2012). The SST pattern is scaled to a global mean of 4 K so that both UNI and PAT experience the same global-mean SST increase. In contrast to UNI, however, PAT includes changes in the SST gradients as represented in the CMIP3 multimodel mean. Thus, the SST impact derived from the PAT simulations implicitly includes the surface pathway of the cloud-radiative heating. Figure 1 (right panel) shows the anomalous annual-mean SST pattern used in PAT. Compared to the uniform 4 K SST increase, the SST increase in PAT is about 1–2 K larger in the Tropics, the northern North Pacific, and the Barents Sea. At the same time, SST is hardly increased south of Greenland (subpolar gyre), in the Southern Ocean, and in the eastern South Pacific.

To isolate the effect of increased SST, sea ice is set to control values in all simulations, and atmospheric greenhouse gas concentrations are kept constant (CO_2 = 390 ppmv, CH_4 = 1,800 ppbv, N_2O = 322 ppbv, CFC_{11} = 240 pptv, CFC_{12} = 532 pptv). We use the GEMS (Global and Regional Earth-System Monitoring using Satellite and In Situ Data; Hollingsworth et al., 2008) ozone climatology from the European Centre for Medium-Range Weather Forecast Integrated Forecast System model. Aerosols are specified according to Tegen et al. (1997). For every simulation, we run the model for 31 years, with the first year being excluded from the analysis to avoid model initialization effects.

We quantify the midlatitude circulation and its response to global warming based on the midlatitude jet streams and storm tracks. Following Barnes and Polvani (2013), we define the latitude and strength of the midlatitude jet streams based on the maximum zonal wind at 850 hPa, u_{850}. In the Northern (Southern) Hemisphere, we search for the maximum u_{850} between 25° N and 70° N (25° S and 70° S) and perform a quadratic fit around the maximum and its two neighboring grid points on an interpolated 0.01° latitude grid. The maximum of the quadratic fit yields the jet strength, u_{jet}, and its position of the jet latitude, φ_{jet}. For ocean-basin mean values of the jet and its response to global warming, the calculation of the jet latitude and jet strength is based on the zonal-mean u_{850} field over the longitudinal boundaries of the respective ocean basin (see below for definition of boundaries). For maps of the u_{850} response shown in section 3, φ_{jet} is calculated at each longitude. To make the comparison between the two hemispheres easier, all latitudes for the Northern Hemisphere are shown in "degrees North" and all latitudes for the Southern Hemisphere in "degrees South". Thus, for both hemispheres, a positive change in φ_{jet} indicates a poleward jet shift.

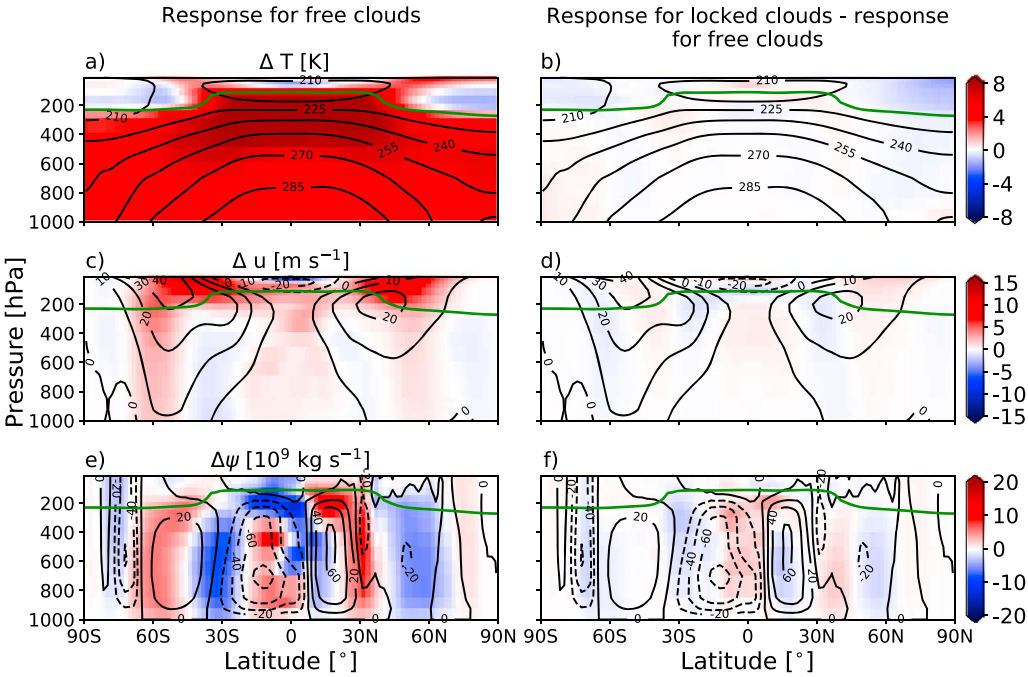

Figure 2. Response of the annual-mean zonal-mean atmospheric temperature (a), zonal wind (c), and mass stream function (e) to a uniform sea surface temperature increase with free clouds (UNI-CTL). The right column (b, d, f) shows the difference between the response in the locked and free simulations. The green line in each panel shows the tropopause height in the control simulation CTL.

We further characterize the storm tracks, which measure the synoptic activity of the midlatitude atmosphere (e.g., Christoph et al., 1995; Chang et al., 2002; Hoskins & Valdes, 1990; Pinto et al., 2007; Shaw et al., 2016; Ulbrich et al., 2008; Yin, 2005). While their magnitude and variability are dominated by transient low pressure systems, they also contain some variability associated with high pressure systems (which typically have longer time scales). We calculate the storm tracks from the standard deviation of the 2.5- to 6-day band-pass filtered 500-hPa geopotential height field (e.g., Blackmon, 1976), using the band-pass filter of the Climate Data Operators (version 1.9.4., available at https://www.mpimet.mpg.de/cdo).

We focus our analysis on the three major ocean basins of the Earth. These are the North Atlantic (60° W–0°), the North Pacific (135°E–125° W), and the Southern Hemisphere Ocean (all longitudes). The longitudinal boundaries of the ocean basins are the same as in Barnes and Polvani (2013).

The left column of Figure 2 shows the global-warming response of the annual-mean zonal-mean circulation in UNI. The model simulates the changes expected from global coupled atmosphere-ocean models (e.g., Grise & Polvani, 2014b; Harvey et al., 2015; Lu et al., 2008; Ma & Xie, 2013). This includes amplified upper-tropospheric warming in the tropics (Figure 2a) and a vertical expansion of the troposphere, which manifests in upward shifts of the upper-level jet streams (Figure 2c) and the upper boundary of the Hadley cells (Figure 2e). ICON also simulates a weakening and horizontal expansion of the tropics, which are indicated by a poleward shift of the midlatitude jet streams in the lower and middle troposphere (Figure 2c) and a weakening and poleward expansion of the Hadley cells (Figure 2e). Very similar results are also found in the PAT simulation (supporting information Figure S1). Note, however, that the Southern Hemisphere Hadley cell strengthens in the PAT simulation. The zonal-mean zonal wind response in our model is consistent with the annual-mean zonal-mean zonal wind response in atmosphere global climate models with fixed SST, in which global warming is mimicked by the spatially varying SST increase of the CMIP5 AmipFuture setup (e.g., cf. Figures 2c and S1c to Figure 5, right panel, in Grise & Polvani, 2014b).

2.2. Cloud-Locking Method

We use the cloud-locking method to quantify the impact of cloud-radiative changes on the response of the midlatitude circulation to global warming. The method allows us to break the radiative interactions and feedbacks between clouds and the circulation by prescribing the radiative properties of clouds to the model's

radiative transfer scheme (e.g., Voigt & Shaw, 2015). While originally devised to study the impact of radiative feedbacks on global-mean and regional surface warming (e.g., Langen et al., 2012; Mauritsen et al., 2013; Schneider et al., 1999; Wetherald & Manabe, 1988), the locking method has become a helpful tool to investigate the contribution of cloud-radiative changes to circulation changes (Ceppi & Hartmann, 2016; Voigt & Shaw, 2015, 2016; Voigt et al., 2019).

In a first step, we diagnose the instantaneous cloud-radiative properties (i.e., cloud water, cloud ice, and cloud fraction) in the CTL, UNI, and PAT simulations. Because cloud-radiative effects are nonlinear functions of cloud-radiative properties, we store the latter at every call of the radiative transfer scheme (every 36 min), as was done in previous studies (e.g., Ceppi & Hartmann, 2016; Voigt & Shaw, 2015). We store 10 years of cloud data to adequately sample cloud variability.

In a next step, we simulate 30 years with cloud-radiative properties prescribed to values from CTL, UNI, or PAT. We cycle three times through the 10 years of stored cloud fields. We have checked that this does not introduce any spurious periodicity to the midlatitude circulation in the prescribed-clouds simulations. The "cloud locking" only affects the radiative transfer scheme. All other components of ICON use the internally simulated clouds. The prescribed cloud-radiative properties are offset by at least 1 year relative to the simulated climate of the model to achieve a spatiotemporal decorrelation of the cloud-radiative properties and the atmospheric circulation, temperature, and moisture. This decorrelation might result in situations in which a cloud-free subsidence region is simulated by the model, but the radiation scheme is run with cloud-radiative properties of a deep convective cloud at the same time. The impact of this decorrelation on the climatological circulation is found to be mainly small in our simulations. This is in line with other studies that used the cloud-locking method to investigate the circulation response to global warming (Ceppi & Hartmann, 2016; Ceppi & Shepherd, 2017; Voigt & Shaw, 2015, 2016; Voigt et al., 2019).

To quantify the cloud-radiative contribution to the circulation change in the UNI simulation, we perform the four additional simulations: T1C1, T1C2, T2C1, and T2C2. The numbers indicate whether SST (T) and cloud-radiative properties (C) are prescribed to values from CTL (simulation 1) or UNI (simulation 2). With this, we decompose the circulation response into a contribution from the SST increase, assuming no changes in the cloud-radiative properties, and a contribution from changes in the cloud-radiative properties assuming no SST increase. The total response of any given variable X to the combined effect of a uniform SST increase and cloud-radiative changes is given by

$$\Delta X = X_{\mathrm{UNI}} - X_{\mathrm{CTL}} = X_{\mathrm{T2C2}} - X_{\mathrm{T1C1}} + Res, \tag{1}$$

where X_{UNI} and X_{CTL} denote the simulations with free clouds and Res is the residual due to the application of the cloud-locking method (see below for more explanations).

The contribution of the SST increase is given by

$$\Delta X_{\mathrm{SST}} = \frac{1}{2}\left[\left(X_{\mathrm{T2C1}} - X_{\mathrm{T1C1}}\right) + \left(X_{\mathrm{T2C2}} - X_{\mathrm{T1C2}}\right)\right] \tag{2}$$

and is referred to as "SST impact" hereafter. Analogously, the contribution of cloud-radiative changes, hereafter referred to as "cloud-radiative impact," is given by

$$\Delta X_{\mathrm{clouds}} = \frac{1}{2}\left[\left(X_{\mathrm{T1C2}} - X_{\mathrm{T1C1}}\right) + \left(X_{\mathrm{T2C2}} - X_{\mathrm{T2C1}}\right)\right]. \tag{3}$$

By construction, the SST and cloud-radiative impact sum up to $X_{\mathrm{T2C2}} - X_{\mathrm{T1C1}}$, so that $\Delta X = \Delta X_{\mathrm{SST}} + \Delta X_{\mathrm{clouds}} + Res$. The cloud-radiative impact in the PAT simulation is quantified in an analogous manner.

Importantly, the residual Res in general is found to be much smaller than ΔX. This can be verified by comparing CTL and UNI with "free" clouds to their "locked" counterparts T1C1 and T2C2, for which the prescribed cloud-radiative properties are decorrelated from the circulation (Figure 2, right). The fact that the residual Res of the locking method is small implies that the locking method can be used to meaningfully separate SST and cloud-radiative impacts.

While the zonal-mean circulation and jet stream responses to global warming in the North Pacific and Southern Hemisphere are similar in the simulations with free and locked clouds, larger differences occur for the jet response over the North Atlantic in the annual mean and during boreal winter (December to February

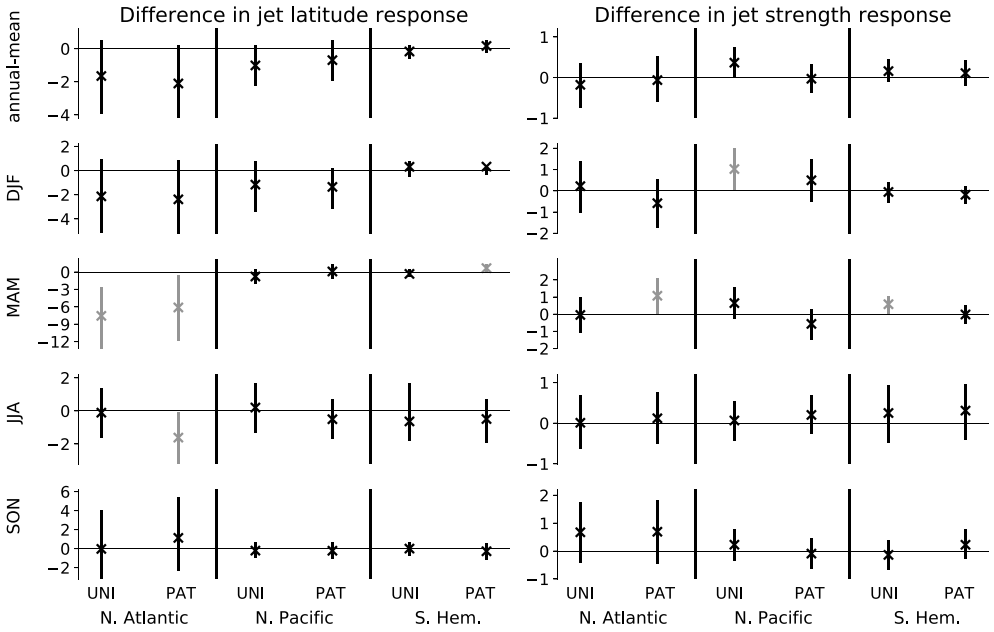

Figure 3. Mean (crosses) and 95% significance level (vertical lines) for the difference in the jet latitude (left) and jet strength (right) responses between simulations with free clouds and simulations with locked clouds. Results are shown for each season, ocean basin, and global warming setup. Black symbols indicate that the responses in simulations with locked and free clouds are statistically similar; gray symbols indicate that they are not statistically similar on a 95% level. Note the different ranges for the vertical axes of the panels.

[DJF]) and spring (March to May [MAM]; Figure S2). During these seasons, the North Atlantic jet stream of the control simulation is located more equatorward for locked clouds than for free clouds. This is possibly related to decreased convective activity over the Maritime Continent and western tropical Pacific when clouds are locked, as indicated by increased outgoing longwave radiation and decreased high-level cloud cover (not shown; e.g., Cassou, 2008; Henderson et al., 2016). At the same time, the North Atlantic jet stream of the UNI and PAT simulations is located more poleward when clouds are locked. This is possibly related to enhanced warming of North America in the simulations with locked clouds (not shown; Ceppi et al., 2018). As a result, in these seasons, the North Atlantic jet shift in the locked simulations is larger than in the free simulations and larger than what is commonly simulated by coupled climate models. However, we are mainly interested in quantifying the impact of cloud-radiative changes in relation to the total (locked) response. Also, the magnitude of the cloud-radiative impact appears to be less sensitive to the jet position in the control simulation. This can be seen by comparing the cloud-radiative impact for each ocean basin across seasons (see section 4). Although the seasons differ with respect to the control jet position (Figure S2), the cloud-radiative impact is similar across seasons, especially in the Northern Hemisphere (see section 4 for a more detailed discussion of the results).

The residual between the jet responses in the simulations with free and locked clouds can either be caused by internal variability or by the decorrelation due to the application of the cloud-locking method. To check that the difference between the simulations is a result of the large internal variability and to verify that the ocean basin mean jet stream responses with free and locked clouds are statistically similar, we analyze their difference for the annual mean and each season. To this end, we calculate the bootstrap distributions for the difference between the jet responses in the simulations with free and locked clouds (see Text S1 and Figure S3 for a more detailed description of the methodology). Figure 3 shows the mean difference between the jet responses in the free and locked simulations for both global warming setups in each ocean basin and season. In the North Pacific and Southern Hemisphere, the jet latitude and jet strength responses are statistically similar on a 95% significance level and close to zero during most seasons. In the North Atlantic, however, large differences between the jet latitude response in the free and locked simulations occur in the annual mean, DJF, and MAM. The largest differences are present in MAM, pointing to a decorrelation effect due to the application of the cloud-locking method in this season. Thus, the results for the jet latitude response in MAM should be interpreted with caution.

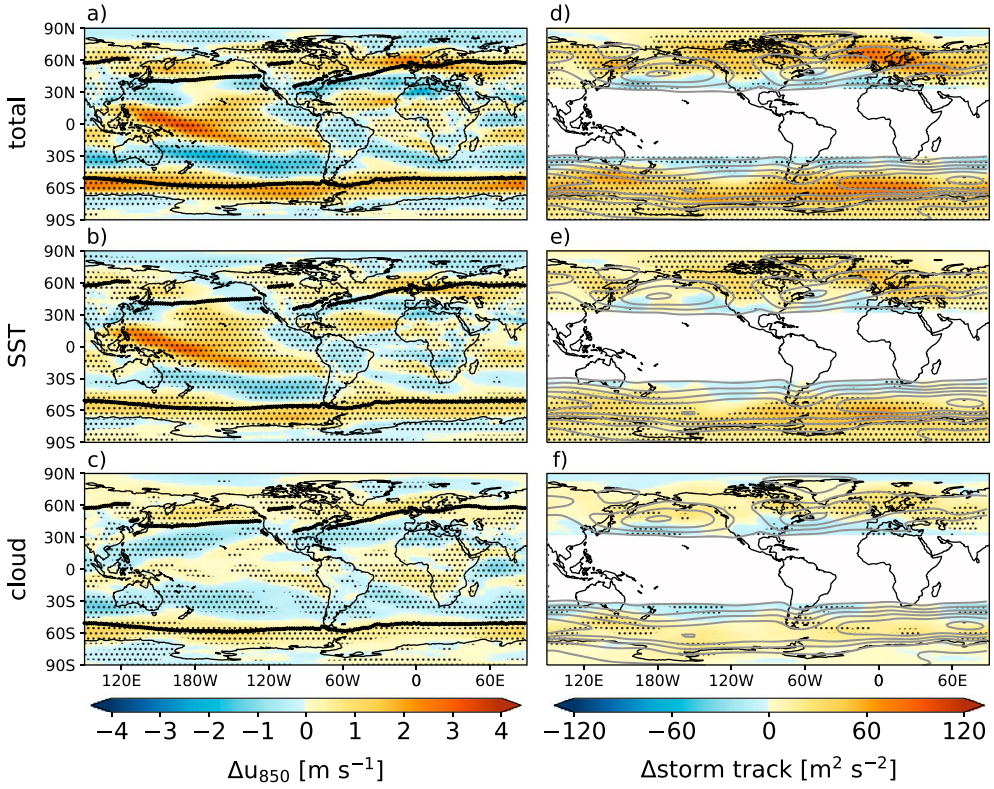

Figure 4. Annual-mean response of the 850-hPa zonal wind, u_{850}, (left) and storm track (right) in the UNI simulations. The total response (a,d) is decomposed into the SST impact (b,e) and the cloud-radiative impact (c,f). The black line in the left column indicates the jet latitude in the control simulation; the gray contours in the right column show the storm track in the control simulation (contour interval of 100 m^2/s^2). For the storm track, the Tropics are not shown. The dots indicate where the response is significant at 95% level.

We have shown that the residual between the jet responses in the simulations with free and locked clouds is small and that the jet response in the simulations with free and locked clouds are statistically similar during most seasons and ocean basins. In the following sections, we will show the results for the simulations with locked clouds, so that the SST impact and cloud-radiative impact sum up to the total response.

2.3. Change in Cloud-Radiative Heating

We perform a forward Partial-Radiative Perturbation (PRP) calculation (Wetherald & Manabe, 1988) to diagnose the change in cloud-radiative heating due to cloud-radiative changes between the CTL and UNI simulations and between the CTL and PAT simulations. The change in cloud-radiative heating is calculated by contrasting the radiative heating rates from CTL with those derived by prescribing UNI or PAT clouds to an atmosphere with otherwise CTL properties. Thus, the change in cloud-radiative heating $\partial T/\partial t$ is given by

$$\left.\frac{\partial T(\varphi,\vartheta,p)}{\partial t}\right|_{\mathrm{PRP}} = R(T_{\mathrm{CTL}}, q_{\mathrm{CTL}}, c_{\mathrm{UNI/PAT}}) - R(T_{\mathrm{CTL}}, q_{\mathrm{CTL}}, c_{\mathrm{CTL}}), \tag{4}$$

where R is the radiative heating rate and T, q, and c are atmospheric temperature, specific humidity, and cloud-radiative properties at latitude φ, longitude ϑ, and pressure p. The subscripts CTL and UNI/PAT indicate whether the variables are taken from the control and global-warming simulations, respectively. The change in cloud-radiative heating is calculated for every grid point at every call of the radiation scheme for a 5-year period.

3. Annual-Mean Circulation Response

In this section, we study the annual-mean response of the midlatitude circulation in the UNI and PAT simulations based on the total response in the prescribed-clouds setup and the decomposition of the response into a cloud-radiative impact and an SST impact. The zonal wind at 850 hPa and the storm tracks undergo significant changes in response to both a uniform (Figures 4a and 4d) and a patterned SST increase (Figures 5a

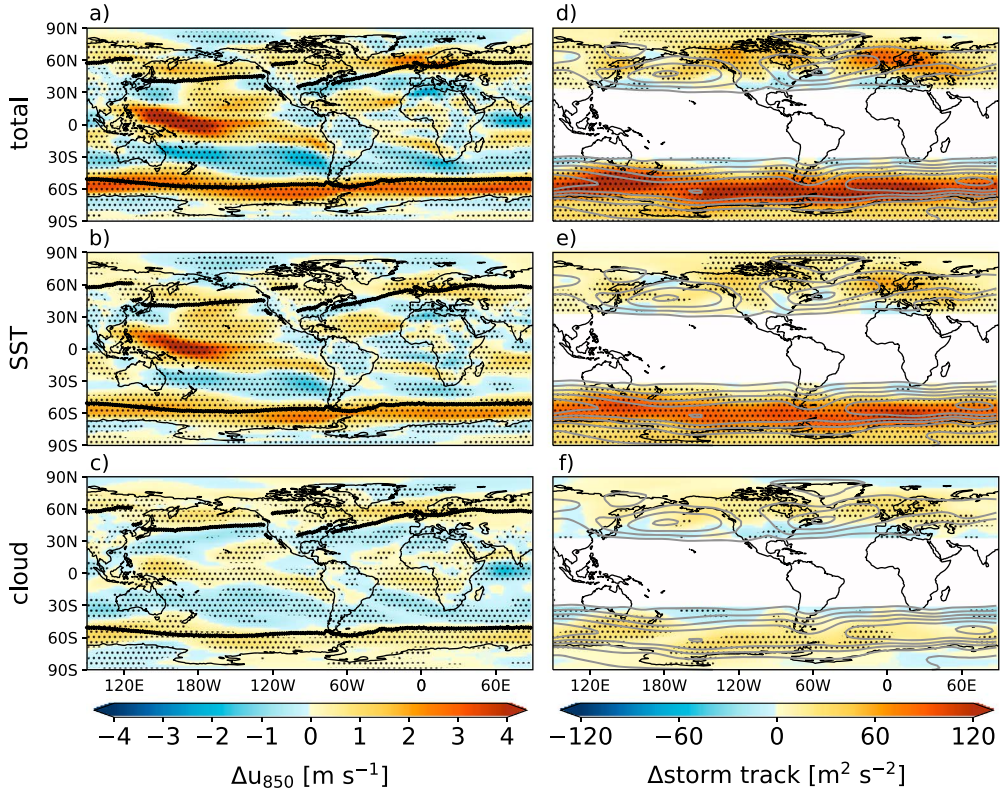

Figure 5. Same as Figure 4 but for the PAT simulations.

and 5d). For the zonal wind shown in the left panels, the black lines indicate the control jet latitude. In the right panels, the gray contours show the storm track in the control simulation. Statistical significance of the responses is indicated by dots and is calculated with a two-sided t test for two samples and using a p value of 0.05 (95% confidence interval).

We have verified that the annual-mean total responses in UNI and PAT are in line with the robust responses in the CMIP5 Amip4 K and AmipFuture simulations (Figures S4 and S5, top rows; Grise & Polvani, 2014b). Differences to the robust annual-mean responses in the CMIP5 models occur mainly in the eastern North Pacific where ICON shows a poleward jet shift, whereas the CMIP5 models show a weakening of the jet and in the Southern Hemisphere east of South America (in UNI) where ICON shows a jet strengthening and the CMIP5 models show a poleward shift. These differences result in a slightly overestimated annual-mean poleward jet shift in the North Pacific and reduced poleward jet shift in the Southern Hemisphere in both global warming setups (Figures S6 and S7).

Figure 4a shows the total response in the UNI simulations. In the North Pacific, changes in u_{850} indicate a poleward jet shift in the western and eastern parts of the ocean basin and a strengthening in the central part. In the North Atlantic, the wind response is more zonal, with a poleward jet shift across the ocean basin and a strengthening in the jet exit region over Europe. In the Southern Hemisphere, the jet exhibits a poleward shift at most longitudes and a strengthening south of Australia and southeast of South America.

Decomposing the total response into SST and cloud-radiative impacts reveals that in all three ocean basins, a substantial part of the midlatitude zonal wind response, and hence jet shift, is attributed to the cloud-radiative impact (Figure 4c). Remarkably, the cloud-radiative impact is almost zonally symmetric in all three ocean basins. In contrast, the SST impact is much more zonally asymmetric (Figure 4b). For example, the jet strengthening over Europe results from the SST impact.

The total storm track response is in line with the total u_{850} response (Figure 4d). The storm track exhibits a poleward shift in the North Pacific and a poleward shift in the North Atlantic with a strengthening in the exit region over Europe. In the Southern Hemisphere, the storm track strengthens at most longitudes, with decreased storm activity on its equatorward flank. This total storm track response is consistent with Ulbrich

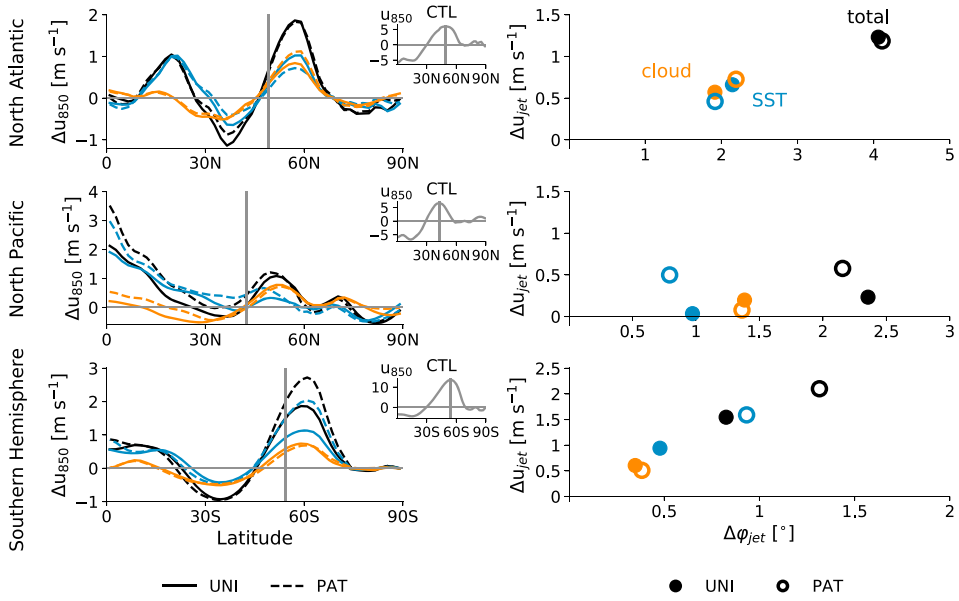

Figure 6. The left panels show the annual-mean response of ocean basin zonal-mean u_{850} in UNI (straight lines) and PAT (dashed lines). The gray bars indicate the jet latitude in CTL derived from the maximum in u_{850} (small inserted figures). The right panels show the poleward jet shift $\Delta\varphi_{\text{jet}}$ versus jet strengthening Δu_{jet}. Results are shown for the North Atlantic (top), North Pacific (middle), and Southern Hemisphere (bottom). The total locked response (black) is decomposed into cloud-radiative impact (orange) and SST impact (blue).

et al. (2009). As for u_{850}, the cloud-radiative impact is nearly zonally symmetric in all three ocean basins (Figure 4f). The cloud-radiative impact dominates the poleward storm track shift in the North Pacific and is strong in the North Atlantic and over Europe. As for u_{850}, the SST impact on the storm track response shows a more complicated spatial structure (Figure 4e).

Figure 5 shows the analogous responses in the PAT simulations. Using a patterned instead of a uniform SST increase leads to a somewhat larger total response and SST impact in the North Pacific and Southern Hemisphere for both the u_{850} and storm track responses (also see Figure S8). In the North Atlantic, the total response and SST impact are slightly reduced for u_{850} and increased in the exit region of the storm track. The cloud-radiative impact on the zonal wind and storm track responses, in contrast, is very similar between the PAT and UNI simulations in all ocean basins.

To allow for a more quantitative analysis, we quantify the response of the jet latitude and jet strength by calculating the zonal-mean u_{850} response over the three ocean basins, using the longitudinal sectors given in section 2. Figure 6 shows the ocean-basin zonal-mean u_{850} response and the associated poleward jet shift and jet strengthening. u_{850} of CTL is shown in small insets for reference. The u_{850} response shows a dipole pattern around the control jet latitude (gray bars in Figure 6, left), with a less pronounced dipole in the North Pacific than in the other two ocean basins. The dipole pattern is found for the total response, the SST impact, and the cloud-radiative impact and is consistent with a poleward jet shift in all three ocean basins and a jet strengthening in the North Atlantic and Southern Hemisphere (Figure 6, right). In the North Atlantic and Southern Hemisphere, an almost linear relationship between the poleward jet shift and the jet strengthening is found.

The cloud-radiative impact on the jet response, measured in absolute values, is very similar in UNI and PAT. This shows that in all three ocean basins, the cloud-radiative impact is largely independent of the spatial pattern of SST increase. At the same time, the relative importance of the cloud-radiative impact is modulated by the pattern of SST increase in the Southern Hemisphere. In the Southern Hemisphere, the cloud-radiative impact contributes more than one third to the jet response in UNI but less than one third in PAT. This results from a stronger total response and stronger SST impact in PAT compared to UNI, consistent with increased SST gradients (see Figure 1). In the North Pacific, the jet strengthening is slightly enhanced in PAT compared to UNI. At the same time, the pattern of SST increase has little or no impact on the jet strength response in the North Atlantic and on the jet latitude response in both ocean basins. In both ocean basins, about half

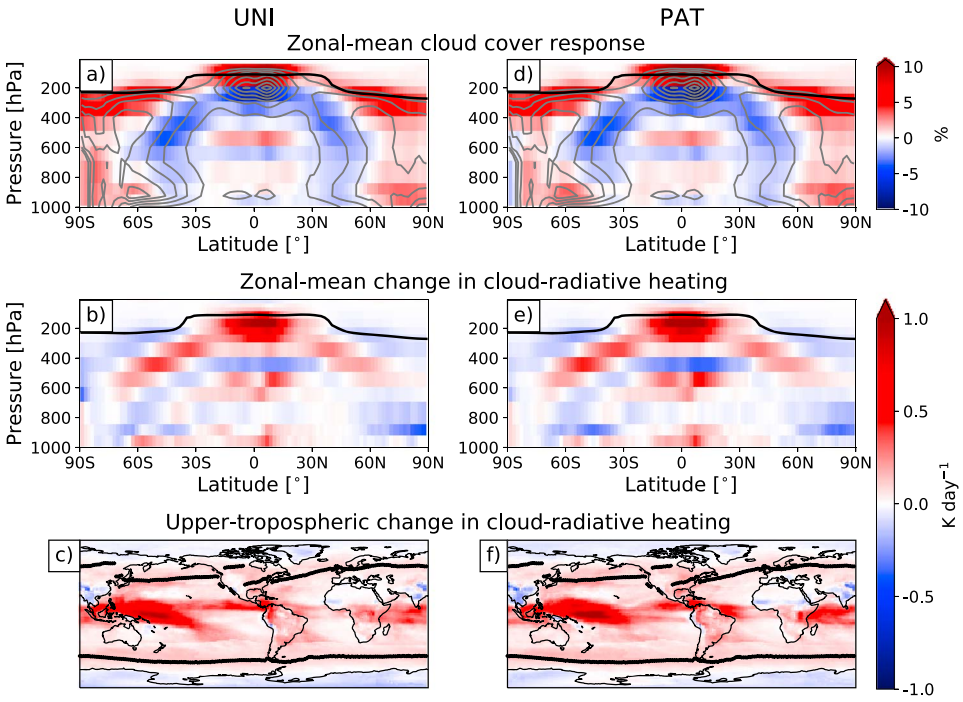

Figure 7. Annual-mean zonal-mean response of cloud cover in the simulations with free clouds (a,d) and annual-mean zonal-mean change in cloud-radiative heating (b,e). The bottom panels (c,f) depict the vertical-mean changes in cloud-radiative heating for a 300-hPa-thick layer below the tropopause. Results are shown for the UNI (left) and PAT (right) simulations. The black lines in the zonal-mean responses indicate the tropopause height in the control simulation; the black line in the maps shows the jet latitude in the control simulation.

to two thirds of the poleward jet shift can be attributed to the cloud-radiative impact for UNI and PAT. In addition, the cloud-radiative impact contributes half to the jet strengthening in the North Atlantic for both UNI and PAT.

The above analysis shows that cloud-radiative changes contribute substantially to the circulation response independent of the pattern of surface warming and that the cloud-radiative impact is nearly zonally symmetric. To understand this, Figure 7 shows cloud cover changes and changes in cloud-radiative heating in the UNI and PAT simulations. The cloud cover changes and cloud-radiative heating changes are consistent with the vertical expansion of the troposphere and poleward expansion of the Tropics shown in Figure 2 and with the fixed anvil temperature hypothesis, which states that high-level clouds rise in response to increased tropospheric temperatures to maintain their cloud-top temperature (Hartmann & Larson, 2002; Thompson et al., 2017). With high-level clouds warming at their base and cooling at their top (see also Li & Thompson, 2016; Slingo & Slingo, 1988), the cloud rise leads to positive changes in cloud-radiative heating in the tropical and midlatitude upper troposphere. The stronger tropical SST increase in PAT compared to UNI leads to a slightly larger change in cloud-radiative heating in the tropical upper troposphere (Figure S9), but overall, the cloud-radiative heating change is very similar between UNI and PAT. A very similar pattern of cloud-radiative heating changes was previously found in aquaplanet simulations in which global warming was mimicked by a uniform 4 K SST increase (Figures 2c and 2d in Voigt & Shaw, 2016) and in present-day simulations in a slab ocean setup under quadrupling of atmospheric CO_2 (Figure 2b of Voigt et al., 2019). Additionally, the pattern is consistent with the atmospheric cloud-radiative heating changes derived from present-day COOKIE simulations (Figure 4b in Li et al., 2019). This supports the idea that the changes in cloud-radiative heating and, thus, the cloud-radiative impact do not strongly depend on the details of surface warming.

Because our simulations include zonal asymmetries from continents, we further investigate the zonal structure of the changes in cloud-radiative heating. The largest changes in cloud-radiative heating are located in the upper troposphere. We therefore analyze the vertical-mean changes in cloud-radiative heating for a 300-hPa-thick layer below the tropopause (Figures 7c and 7f). In the midlatitudes of both hemispheres,

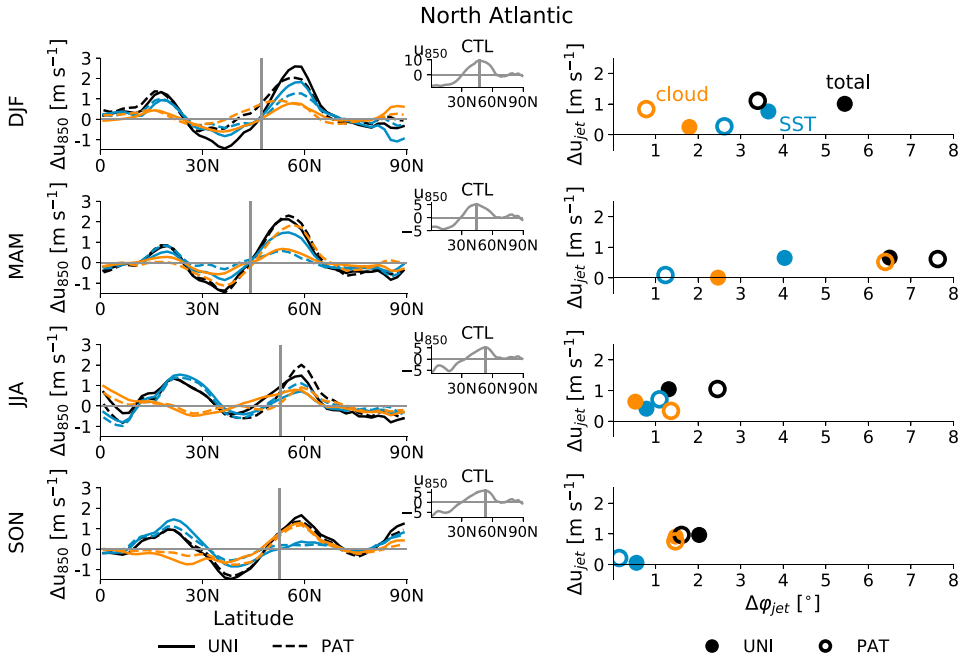

Figure 8. Seasonal-mean response of the ocean basin zonal-mean u_{850} response to a uniform (straight line) and patterned (dashed line) SST increase (left) in the North Atlantic. The gray bar indicates the jet latitude in the control simulation derived from the maximum in u_{850} (small inserted figures). The right panel shows the poleward jet shift $\Delta\varphi_{\text{jet}}$ versus the jet strengthening Δu_{jet}. The total locked response (black) is decomposed into cloud-radiative impact (orange) and SST impact (blue).

the changes in cloud-radiative heating are zonally symmetric and exhibit a similar magnitude in both global warming setups (Figure S9). This is consistent with the zonally symmetric cloud-radiative impact in Figures 4 and 5, which also exhibits similar magnitudes in both global warming setups. Zonal asymmetries in the cloud-radiative heating changes are found in the Tropics, especially in the regions of deep convection over the western Pacific and the Indian Ocean (Figures 7c and 7f). This region also shows the largest change in cloud-radiative heating. Because increased convection over this region can affect the jet latitude in the North Atlantic (e.g., Cassou, 2008; Henderson et al., 2016), we expect that the large change in cloud-radiative heating modifies the jet response in the North Atlantic. However, even though UNI and PAT exhibit different patterns of the upper-tropospheric change in cloud-radiative heating, the cloud-radiative impact on the North Atlantic jet stream response is similar in both global warming setups. This indicates that the small-scale structure of the change in cloud-radiative heating might be less important than its location in the western tropical Pacific.

4. Seasonal-Mean Circulation Response

In this section, we investigate the cloud-radiative impact on the seasonal-mean jet stream response and compare it to the annual-mean response. As in section 3, we base our analysis on the total response in the prescribed-clouds setup and its decomposition into a cloud-radiative impact and an SST impact. To this end, Figures 8-10 show the seasonal-mean wind and jet responses separately for each ocean basin. As for the annual mean, an almost linear relationship between the poleward jet shift and jet strengthening is found in all three ocean basins during seasons which exhibit both the jet shift and jet strengthening. The linear behavior is most strongly pronounced in the Southern Hemisphere during DJF and MAM.

As for the annual mean, the seasonal-mean total zonal wind responses in UNI and PAT reproduce most of the robust zonal wind responses of the CMIP5 Amip4 K and AmipFuture simulations (Figures S4 and S5, second to fifth rows). The largest differences compared to the robust response in the CMIP5 models occur in the North Pacific during DJF and MAM. In DJF, ICON does not reproduce the equatorward jet shift in the eastern part of the North Pacific. In MAM, ICON simulates a poleward shift in the North Pacific, whereas the CMIP5 models show a jet strengthening. In the Southern Hemisphere, ICON shows a jet strengthening east of South America in JJA and SON, whereas most of the CMIP5 models show a poleward shift in this

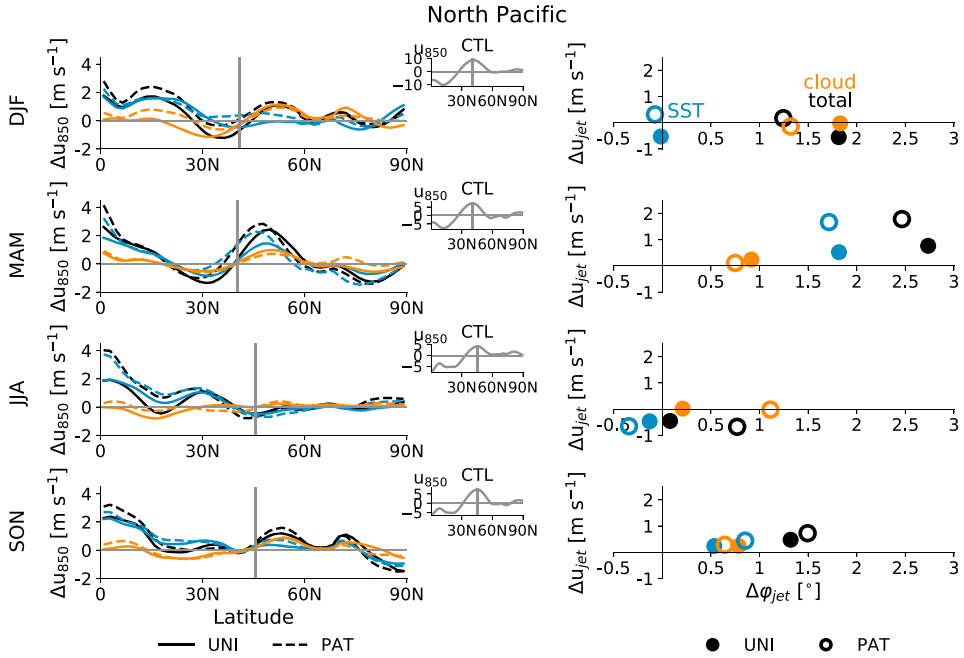

Figure 9. Same as Figure 8 but for the North Pacific.

region. The ocean basin mean jet responses in ICON are within the range of the CMIP5 models during most of the seasons and for all three ocean basins (Figures S6 and S7), although ICON shows a comparably small poleward shift of the Southern Hemisphere jet in DJF and MAM and little jet responses in JJA and SON, as well as a comparably large jet shift in the North Pacific during MAM.

In the North Atlantic, the cloud-radiative impact supports the poleward jet shift in UNI and PAT during all seasons (Figure 8). It contributes to the jet strengthening in JJA and SON for the UNI simulations and during all seasons for the PAT simulations. With respect to the jet shift, the cloud-radiative impact exhibits only a small seasonal cycle and is of similar magnitude as in the annual mean (cf. Figure 8 to top row of Figure 6), except for MAM in the PAT simulations for reasons that are unknown to us. As in the annual mean and with the exception of MAM, the seasonal-mean cloud-radiative impact is largely independent of the SST pattern. In contrast, the total jet shift and the SST impact exhibit distinct seasonal cycles. This leads to strong seasonal variations of the relative importance of the cloud-radiative impact. The relative importance of the cloud-radiative impact can range from about a quarter (during DJF in PAT) to almost all of the poleward jet shift (during SON in PAT). With respect to the jet strength, the seasonal cycles of the total response, the cloud-radiative impact, and the SST impact are of similar magnitude. In the UNI simulations, the relative importance of the cloud-radiative impact on the jet strength varies between seasons. In the PAT simulations, more than three quarters of the total jet strength response can be attributed to the cloud-radiative impact (except JJA).

In the North Pacific, the cloud-radiative impact leads to a poleward jet shift in all seasons while having essentially no impact on the seasonal jet strength response (Figure 9). Apart from JJA, the cloud-radiative impact on the jet latitude response is mostly independent of the SST pattern, consistent with the annual-mean response (Figure 6, middle row). In terms of relative importance, the cloud-radiative impact contributes between about one third to the jet shift during MAM and is in fact larger than the total response during JJA. The strong seasonal cycle in the relative importance reflects the strong seasonal cycle of the SST impact, which contributes to a poleward jet shift in MAM but tends to lead to an equatorward shift in JJA. We note that the equatorward shift and weakening of the jet during JJA likely arises from negative land-sea equivalent potential temperature contrasts when SST are warmed, but atmospheric CO_2 is kept at the present-day level (Shaw & Voigt, 2015).

In the Southern Hemisphere, the four seasons can be arranged into two groups according to the simulated jet shifts (Figure 10). The first group consists of DJF and MAM, for which the jet shifts poleward, similar to the

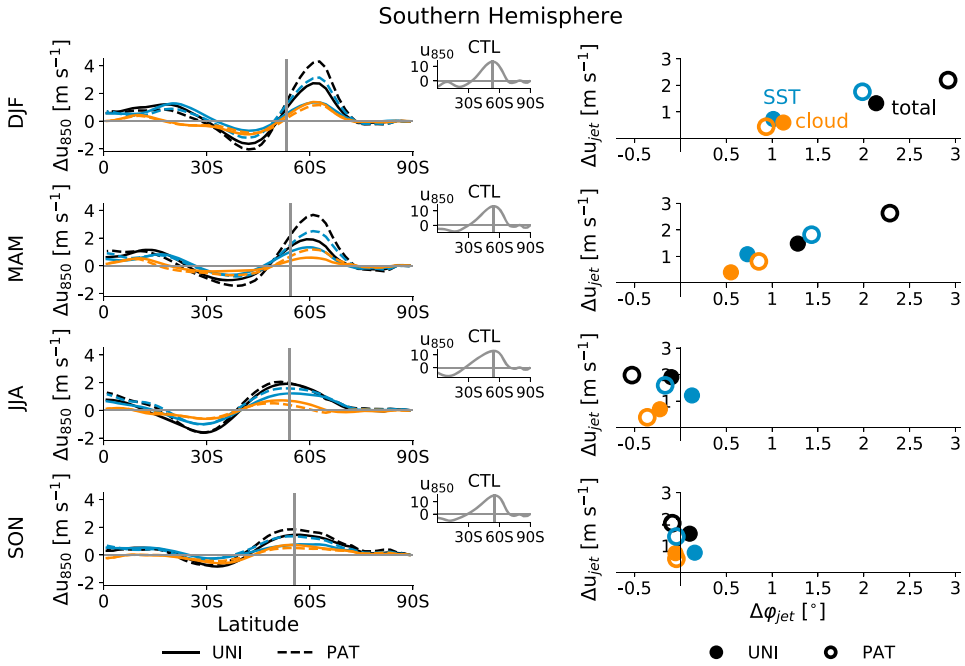

Figure 10. Same as Figure 8 but for the Southern Hemisphere.

annual mean (cf. Figure 10 to lower row of Figure 6). The cloud-radiative impact is of similar magnitude during both seasons and for both global warming setups. At the same time, the increased SST gradients in PAT lead to a much stronger SST impact compared to UNI, so that the relative importance of the cloud-radiative impact ranges between about one third (during DJF in PAT) and more than half (during DJF in UNI) of the total jet shift. The second group consists of SON and JJA, for which the total jet shift is small or even slightly equatorward, independent of the pattern of SST increase. The slight equatorward shift during JJA is supported by the cloud-radiative impact, while in SON, the jet latitude hardly responds to global warming, and the cloud-radiative impact is negligible. In contrast to seasonally dependent changes in its position, the jet becomes stronger in all four seasons. The cloud-radiative impact on the jet strengthening is of similar magnitude during all seasons and its relative importance ranges between about one fifth (during DJF and JJA in PAT) and half (during SON in UNI) of the total response.

Figures S10–S12 show maps of the seasonal-mean u_{850} responses in UNI and PAT, as well as the differences between the two global warming setups. As for the annual mean, the seasonal-mean cloud-radiative impact is largely zonally symmetric in all ocean basins and during most seasons, except for JJA. During this season, exceptions of the zonal cloud-radiative impact are found in the North Pacific (in UNI), in the North Atlantic (in PAT), and the Southern Hemisphere (in PAT). Note that during JJA, the cloud-radiative impact is larger than the total jet shift in the North Pacific and counteracted by an almost ocean basin wide equatorward shift due to the SST impact.

To sum up, we have shown that the seasonal-mean cloud-radiative impact is largely zonally symmetric and shows little dependence on the pattern of SST increase during most seasons in all three ocean basins. In the North Atlantic and North Pacific, the cloud-radiative impact varies little over the course of the year and supports the poleward jet shift during all seasons. The relative importance of the cloud-radiative impact depends on the season, because the total response and SST impact exhibit seasonal cycles. A similar result is found for the Southern Hemisphere during DJF and MAM. The cloud-radiative impact supports the jet strengthening in the North Atlantic during JJA and SON for UNI and during all seasons for PAT and contributes to the jet strengthening in the Southern Hemisphere during all seasons.

Table 1
Correlation Coefficients for Linear Correlation Between Ocean Basin Mean Jet Latitude and Upper-Tropospheric Temperature Gradient (a). Panel b shows the same for the jet strength. Correlation coefficients which are significant at a 95% level are shown in bold letters for better visualization of large linear correlations. Positive correlations indicate that increased (decreased) temperature gradients correspond to (a) a more poleward (equatorward) located and (b) a stronger (weaker) jet stream

		Jet latitude	
a)	North Atlantic	North Pacific	Southern Hemisphere
Annual mean	**0.87**	0.74	**0.95**
DJF	0.71	0.19	**0.96**
MAM	0.66	**0.97**	**0.87**
JJA	0.75	−0.09	−0.37
SON	0.58	**0.92**	0.18
b)		**Jet strength**	
	North Atlantic	North Pacific	Southern Hemisphere
Annual mean	0.76	0.76	**0.96**
DJF	0.63	−0.04	**0.90**
MAM	0.45	**0.81**	**0.93**
JJA	**0.89**	**−0.89**	**0.96**
SON	0.58	**0.90**	**0.97**

5. Relations Between the Jet Stream and the Atmospheric Equator-to-Pole Temperature Gradient

In this section, we investigate to what extent the jet stream and its response to global warming are correlated with the upper-tropospheric meridional temperature gradients in all three ocean basins and all seasons. Following Harvey et al. (2014), we calculate the upper-tropospheric (250 hPa) equator-to-pole temperature gradient as the difference between ocean basin zonal mean tropical (30° S–30° N) and polar (poleward of 60° N/S) atmospheric temperatures. We chose this pressure level because in our simulations, the jet stream and the temperature gradient and their responses show higher correlations in the upper troposphere than in the lower troposphere.

In a first step, we investigate to what extent the annual-mean and seasonal-mean jet streams and upper-tropospheric temperature gradients are correlated for different states of the climate system. For this, we use the ocean basin mean jet latitude, jet strength, and equator-to-pole temperature gradient of the seven simulations with locked clouds. These simulations are T1C1, T1C2, T2C1, T2C2, T1C3, T3C1, and T3C3. As described in section 2.2, the numbers indicate whether SST (T) and cloud-radiative properties (C) are prescribed to values from CTL (simulation 1), UNI (simulation 2), or PAT (simulation 3). Figure S13 shows the scatter plots from which the correlation coefficients of Table 1 were derived. The seven simulations are not strongly clustered according to the underlying SST pattern during most seasons and for most of the ocean basins. Thus, the significant correlations between the temperature gradient and jet stream are not driven by the SST increase. In the Southern Hemisphere, the jet latitude and jet strength are significantly correlated with the upper-tropospheric temperature gradient both in the annual-mean and in most seasons (except for JJA and SON for the jet latitude; Table 1). In the North Pacific, the jet stream is significantly correlated with the temperature gradient during MAM and SON. Note that in both ocean basins, negative correlations between the temperature gradient and jet latitude or jet strength are found and are significant in the North Pacific during JJA. The negative correlation during JJA is consistent with the findings of Shaw and Voigt (2015), who showed that ocean warming can result in an equatorward shift of the North Pacific jet in summer. The North Atlantic jet stream is not significantly correlated with the temperature gradient during most seasons. In summary, our results indicate that the upper-tropospheric temperature gradient bears some information for the position and strength of the Southern Hemisphere jet stream but little information for the North Pacific and North Atlantic jet streams.

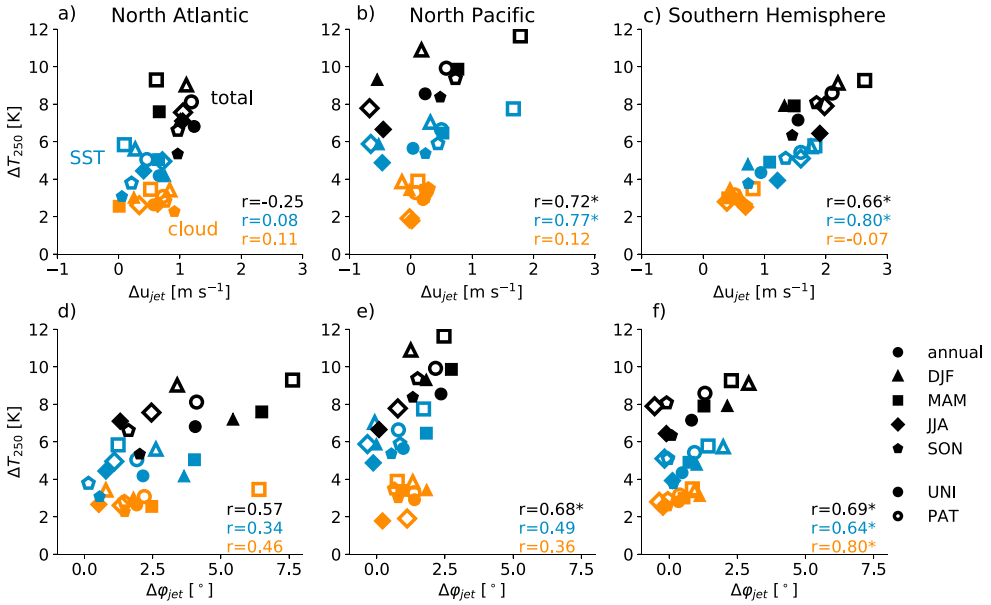

Figure 11. Correlation between temperature gradient response at 250 hPa, ΔT_{250}, and jet strength response, Δu_{jet}, (a–c) and jet latitude response, $\Delta\varphi_{jet}$, (d–f) for the North Atlantic, North Pacific, and Southern Hemisphere. Filled markers are for the response in UNI; open markers for the response in PAT. The total response (black markers) is decomposed into the cloud-radiative impact (orange markers) and the SST impact (blue markers). Correlation coefficients *r* are marked with a star if they are significant on a 95% level.

Previous studies related the global warming response of the midlatitude circulation to changes in upper- and/or lower-tropospheric meridional temperature gradients (e.g., Harvey et al., 2014, 2015; Lorenz & DeWeaver, 2007; Yin, 2005). Thus, in a second step, we investigate whether the cloud-radiative impact on the temperature gradient response in the three ocean basins can be used to infer the cloud-radiative impact on the jet stream response in the respective ocean basin. The idea for this originated from the work of Gerber and Son (2014) who related, and thereby attributed, the jet shift to changes in polar stratospheric temperatures (due to ozone) and changes in tropical upper-tropospheric temperatures (due to greenhouse gases). A similar approach was taken by Ceppi and Shepherd (2017). Here we investigate the relation between the jet response and the temperature gradient response for the SST impact and the cloud-radiative impact. The correlation between the jet stream response and the equator-to-pole temperature gradient response at 250 hPa is shown in Figure 11. In all three ocean basins, the temperature gradient increases in response to global warming in all seasons (Figure 11). At the same time, the jet strengthens and shifts poleward in the North Atlantic and strengthens in the Southern Hemisphere during all seasons. However, as discussed in section 4, during some seasons, the North Pacific jet stream weakens and shifts equatorward, and the Southern Hemisphere jet stream shifts equatorward.

To assess to what extent the temperature gradient response and the jet stream response are correlated, we calculate correlation coefficients individually for the total response, SST impact, and cloud-radiative impact based on the annual-mean and seasonal-mean responses in both UNI and PAT. The cloud-radiative impact shows rather small correlations, except for the jet shift in the Southern Hemisphere (Figure 11). This is due to the fact that the cloud-radiative impact is of similar magnitude over the course of the year and for both global warming simulations. In contrast, the total response and SST impact exhibit distinct seasonal cycles, resulting in significant correlations between the jet response and the temperature gradient response, especially in the Southern Hemisphere and North Pacific. This suggests that in a large model ensemble for which only the total response is available, such as CMIP5/6, the SST impact could be inferred indirectly from the upper-tropospheric temperature response, but the cloud-radiative impact could not. Thus, a proper diagnostic of the cloud-radiative impact requires dedicated cloud-locking simulations.

The fact that we generally could not find a linear correlation for the cloud-radiative impact is in agreement with McGraw and Barnes (2016), who used a dry dynamical model to investigate the jet stream response to a time-constant tropical upper-tropospheric thermal forcing. They found that the temperature response to

the thermal forcing does not exhibit a seasonal cycle, whereas the jet latitude and jet strength responses do exhibit distinct seasonal cycles. As a result, McGraw and Barnes (2016) found no correlation between the jet stream response and the temperature gradient response. This is in line with our results.

6. Discussion and Conclusions

We study the impact of cloud-radiative changes on the global warming responses of the midlatitude jet streams and storm tracks in the North Atlantic, North Pacific, and Southern Hemisphere and determine whether the cloud-radiative impact depends on the ocean basin, season, and pattern of SST increase. For this purpose, we use the atmospheric component of the ICON model and prescribe SST to isolate the impact of cloud-radiative changes via the atmospheric pathway, that is, the impact of changes in atmospheric cloud-radiative heating in the absence of a cloud-radiative impact on ocean surface temperatures (Voigt et al., 2019).

Changes in atmospheric cloud-radiative heating have a substantial impact on the annual-mean jet stream and storm track responses to global warming, with little dependence on the pattern of SST increase. Note that the impact of surface cloud-radiative heating, which is disabled in our simulations, may depend on the pattern of SST increase, because they lead to changes in surface temperatures (Ceppi & Hartmann, 2016; Voigt et al., 2019). The cloud-radiative impact is largely zonally symmetric, consistent with a zonally symmetric change in cloud-radiative heating in the midlatitude upper troposphere. The magnitude of the cloud-radiative impact depends on the ocean basin. In a relative sense, cloud-radiative changes contribute one to two thirds to the annual-mean poleward jet shift in all three ocean basins and support the jet strengthening in the North Atlantic and Southern Hemisphere. Regarding the seasonal jet response, the cloud-radiative impact varies little with seasons in the North Atlantic and North Pacific. Yet, because the total jet stream response and the SST impact exhibit distinct seasonal cycles, the relative importance of the cloud-radiative impact changes over the course of the year. In the Southern Hemisphere, the cloud-radiative impact supports the jet strengthening in all seasons and contributes to the poleward jet shift in austral summer and fall. As for the annual mean, the cloud-radiative impact on the seasonal jet stream response is largely zonally symmetric and depends little on the pattern of SST increase.

Similar to the zonal cloud-radiative impact, the direct radiative impact of CO_2 on the zonal wind response is also largely zonally uniform in present-day simulations of atmospheric general circulation models (Grise & Polvani, 2014b). Grise and Polvani (2014b) also attributed the asymmetries in the total response to changes in the SST, as in our study with the cloud-locking method.

Previous studies investigated the zonal-mean jet stream and storm track responses to global warming in idealized aquaplanet simulations without a seasonal cycle. They found that cloud-radiative changes cause more than half of the zonal-mean near-surface zonal wind (Voigt & Shaw, 2015) and jet latitude responses (Ceppi & Hartmann, 2016) and dominate the storm track response (Ceppi & Hartmann, 2016). Voigt et al. (2019) showed that more than half of the annual-mean zonal-mean jet shift in a present-day setup can be attributed to the atmospheric pathway of the cloud-radiative impact. We extend this prior work and show that the absolute value of the cloud-radiative impact strongly depends on the ocean basin and has only a small seasonal cycle in the Northern Hemisphere. In addition, we show that the relative role of the cloud-radiative impact on the jet stream response varies across ocean basins and seasons. This highlights the importance of the present-day setup, and the investigation of individual ocean basins, for understanding the role of cloud-radiative changes on the midlatitude circulation response to global warming.

While continents are important for the jet stream response in the three ocean basins, the pattern of SST increase plays a minor role for the cloud-radiative impact on the jet stream and storm track responses. In our simulations, the pattern of the SST increase has only a small impact on the absolute value of the cloud-radiative impact in all three ocean basins and across seasons. Thus, the uniform 4 K SST increase provides meaningful estimates of the absolute value of the cloud-radiative impact, although is not able to reproduce the total jet stream response of coupled climate models, especially in the Southern Hemisphere, where the jet strongly responds to changes in SST gradients.

Even though the cloud-radiative impact does not strongly depend on the pattern of SST increase and season in the model used here, previous work indicates that the cloud-radiative impact strongly differs between models. Voigt et al. (2019) showed that the annual-mean zonal-mean change in atmospheric cloud-radiative

heating and, thus, the magnitude of the cloud-radiative impact strongly depend on the model. These model differences arise both from differences in the cloud response as well as differences in the radiation schemes and assumptions regarding the radiative characteristics of ice clouds. Additionally, in coupled climate models, the cloud-radiative impact is a sum of the atmospheric and surface pathways of the change in cloud-radiative heating. The latter might depend on the pattern of SST increase and season.

Finally, we investigated the correlation between the upper-tropospheric temperature gradient response and the jet stream response. For the cloud-radiative impact, increased temperature gradients coincide with a strengthening of the Southern Hemisphere jet stream, while correlations between cloud-induced changes in the temperature gradient and the jet are weak in the Northern Hemisphere. This lack of correlation is a result of the fact that the cloud-radiative impact does not strongly depend on season in the Northern Hemisphere. In contrast, the total response and SST impact exhibit distinct seasonal cycles, resulting in significant linear correlations between the jet stream response and upper-tropospheric temperature gradient response, with statistically significant correlations in the Southern Hemisphere and North Pacific. This also indicates that the cloud-radiative impact on the jet cannot be inferred indirectly from the temperature response but requires cloud-locking simulations.

Our results emphasize the importance of cloud-radiative changes for the global warming response of the midlatitude atmospheric circulation. Previous studies, which focused on the annual-mean zonal-mean cloud-radiative impact, showed that its magnitude differs across models and remains uncertain in both aquaplanet (Voigt & Shaw, 2016) and present-day simulations (Voigt et al., 2019). Thus, future studies should investigate the ocean basin mean circulation response across seasons in a larger model ensemble. This would enable to quantify model differences in representing the change in cloud-radiative heating and its effect on the circulation's response. Finally, we found a particularly large change in cloud-radiative heating over the tropical western Pacific and Indian Ocean, which could be important for the midlatitude circulation response to global warming. We hope to quantify the role of this heating in a future study using regionally prescribed cloud-radiative changes.

Acknowledgments
N. A. and A. V. are supported by the German Ministry of Education and Research (BMBF) and FONA: Research for Sustainable Development (www.fona.de) under grant agreement 01LK1509A. J. G. P. thanks AXA research fund for support. The ICON simulations were carried out by N. A. and A. V. at the Mistral supercomputer of the German Climate Computing Center (DKRZ) in Hamburg, Germany, and are published at KITopen with doi 10.5445/IR/1000094317. This work contributes to the WCRP's Grand Challenge on Clouds, Circulation, and Climate Sensitivity and the BMBF-funded project "HD(CP)^2: High Definition Clouds and Precipitation for Advancing Climate Prediction".

References

Allan, R. P. (2011). Combining satellite data and models to estimate cloud radiative effect at the surface and in the atmosphere. *Meteorological Applications*, *18*(3), 324–333.

Barnes, E. A., & Polvani, L. M. (2013). Response of the midlatitude jets and of their variability to increased greenhouse gases in CMIP5 models. *Journal of Climate*, *26*, 7117–7135.

Blackmon, M. L. (1976). A climatological spectral study of the 500 mb geopotential height of the Northern Hemisphere. *Journal of the Atmospheric Sciences*, *33*(8), 1607–1623.

Bony, S., Stevens, B., Frierson, D. M. W., Jakob, C., Kageyama, M., Pincus, R., et al. (2015). Clouds, circulation and climate sensitivity. *Nature Geoscience*, *8*, 261–268.

Brayshaw, D. J., Hoskins, B. J., & Blackburn, M. (2009). The basic ingredients of the North Atlantic storm track. Part I: Land-sea contrast and orography. *Journal of the Atmospheric Sciences*, *66*(9), 2539–2558.

Butler, A. H., Thompson, D. W., & Heikes, R. (2010). The steady-state atmospheric circulation response to climate change-like thermal forcings in a simple general circulation model. *Journal of Climate*, *23*, 3474–3496. https://doi.org/10.1175/2010JCLI3228.1

Cassou, C. (2008). Intraseasonal interaction between the Madden–Julian oscillation and the North Atlantic Oscillation. *Nature*, *455*(7212), 523–527.

Ceppi, P., & Hartmann, D. L. (2016). Clouds and the atmospheric circulation response to warming. *Journal of Climate*, *29*, 783–799.

Ceppi, P., Hwang, Y.-T., Frierson, D. M. W., & Hartmann, D. L. (2012). Southern Hemisphere jet latitude biases in CMIP5 models linked to shortwave cloud forcing. *Geophysical Research Letters*, *39*, L19708. https://doi.org/10.1029/2012GL053115

Ceppi, P., & Shepherd, T. G. (2017). Contributions of climate feedbacks to changes in atmospheric circulation. *Journal of Climate*, *30*(22), 9097–9118.

Ceppi, P., Zappa, G., Shepherd, T. G., & Gregory, J. M. (2018). Fast and slow components of the extratropical atmospheric circulation response to CO_2 forcing. *Journal of Climate*, *31*(3), 1091–1105. https://doi.org/10.1175/JCLI-D-17-0323.1

Ceppi, P., Zelinka, M. D., & Hartmann, D. L. (2014). The response of the Southern Hemispheric eddy-driven jet to future changes in shortwave radiation in CMIP5. *Geophysical Research Letters*, *41*, 3244–3250. https://doi.org/10.1002/2014GL060043

Chang, E. K. M., Guo, Y., & Xia, X. (2012). CMIP5 multimodel ensemble projection of storm track change under global warming. *Journal of Geophysical Research*, *117*, D23118. https://doi.org/10.1029/2012JD018578

Chang, E. K. M., Lee, S., & Swanson, K. L. (2002). Storm track dynamics. *Journal of Climate*, *15*(16), 2163–2183.

Christoph, M., Ulbrich, U., & Haak, U. (1995). Faster determination of the intraseasonal variability of storm tracks using Murakami's recursive filter. *Monthly Weather Review*, *123*(2), 578–581. https://doi.org/10.1175/1520-0493(1995)123<0578:FDOTIV>2.0.CO;2

Gates, W. L. (1992). AMIP: The Atmospheric Model Intercomparison Project. *Bulletin of the American Meteorological Society*, *73*(12), 1962–1970. https://doi.org/10.1175/1520-0477(1992)073<1962:ATAMIP>2.0.CO;2

Gerber, E. P., & Son, S.-W. (2014). Quantifying the summertime response of the Austral jet stream and Hadley cell to stratospheric ozone and greenhouse gases. *Journal of Climate*, *27*, 5538–5559.

Grise, K. M., & Polvani, L. M. (2014a). Southern Hemisphere cloud-dynamics biases in CMIP5 models and their implications for climate projections. *Journal of Climate*, *27*, 6074–6092.

Grise, K. M., & Polvani, L. M. (2014b). The response of midlatitude jets to increased CO_2: Distinguishing the roles of sea surface temperature and direct radiative forcing. *Geophysical Research Letters*, *41*, 6863–6871. https://doi.org/10.1002/2014GL061638
Hartmann, D. L., & Larson, K. (2002). An important constraint on tropical cloud-climate feedback. *Geophysical Research Letters*, *29*(20), 1951. https://doi.org/10.1029/2002GL015835
Harvey, B. J., Shaffrey, L. C., & Woollings, T. J. (2014). Equator-to-pole temperature differences and the extra-tropical storm track responses of the CMIP5 climate models. *Climate Dynamics*, *43*(5), 1171–1182.
Harvey, B. J., Shaffrey, L. C., & Woollings, T. J. (2015). Deconstructing the climate change response of the Northern Hemisphere wintertime storm tracks. *Climate Dynamics*, *45*(9), 2847–2860. https://doi.org/10.1007/s00382-015-2510-8
Henderson, S., D. Maloney, E., & Barnes, E. (2016). The influence of the Madden-Julian Oscillation on Northern Hemisphere winter blocking. *Journal of Climate*, *29*, 4597–4616.
Hollingsworth, A., Engelen, R. J., Textor, C., Benedetti, A., Boucher, O., Chevallier, F., et al. the GEMS Consortium (2008). Toward a monitoring and forecasting system for atmospheric composition. *Bulletin of the American Meteorological Society*, *89*(8), 1147–1164. https://doi.org/10.1175/2008BAMS2355.1
Hoskins, B. J., & Valdes, P. J. (1990). On the existence of storm-tracks. *Journal of the Atmospheric Sciences*, *47*(15), 1854–1864.
Kushner, P. J., Held, I. M., & Delworth, T. L. (2001). Southern Hemisphere atmospheric circulation response to global warming. *Journal of Climate*, *14*(10), 2238–2249.
Langen, P. L., Graversen, R. G., & Mauritsen, T. (2012). Separation of contributions from radiative feedbacks to polar amplification on an Aquaplanet. *Journal of Climate*, *25*(8), 3010–3024.
Li, Y., & Thompson, D. W. J. (2016). Observed signatures of the barotropic and baroclinic annular modes in cloud vertical structure and cloud radiative effects. *Journal of Climate*, *29*(13), 4723–4740. https://doi.org/10.1175/JCLI-D-15-0692.1
Li, Y., Thompson, D. W. J., & Bony, S. (2015). The influence of atmospheric cloud radiative effects on the large-scale atmospheric circulation. *Journal of Climate*, *8*, 7263–7278.
Li, Y., Thompson, D. W. J., Bony, S., & Merlis, T. M. (2019). Thermodynamic control on the poleward shift of the extratropical jet in climate change simulations: The role of rising high clouds and their radiative effects. *Journal of Climate*, *32*, 917–934.
Lorenz, D. J., & DeWeaver, E. T. (2007). Tropopause height and zonal wind response to global warming in the IPCC scenario integrations. *Journal of Geophysical Research*, *112*, D10119. https://doi.org/10.1029/2006JD008087
Lu, J., Chen, G., & Frierson, D. M. W. (2008). Response of the zonal mean atmospheric circulation to El Nio versus global warming. *Journal of Climate*, *21*(22), 5835–5851.
Ma, J., & Xie, S.-P. (2013). Regional patterns of sea surface temperature change: A source of uncertainty in future projections of precipitation and atmospheric circulation. *Journal of Climate*, *26*(8), 2482–2501.
Mauritsen, T., Graversen, R. G., Klocke, D., Langen, P. L., Stevens, B., & Tomassini, L. (2013). Climate feedback efficiency and synergy. *Climate Dynamics*, *41*, 2539–2554. https://doi.org/10.1007/s00382-013-1808-7
McGraw, M. C., & Barnes, E. A. (2016). Seasonal sensitivity of the eddy-driven jet to tropospheric heating in an idealized AGCM. *Journal of Climate*, *29*(14), 5223–5240.
Pinto, J. G., Spangehl, T., Ulbrich, U., & Speth, P. (2006). Assessment of winter cyclone activity in a transient ECHAM4-OPYC3 GHG experiment. *Meteorologische Zeitschrift*, *15*(3), 279–291. https://doi.org/10.1127/0941-2948/2006/0128
Pinto, J. G., Ulbrich, U., Leckebusch, G. C., Spangehl, T., Reyers, M., & Zacharias, S. (2007). Changes in storm track and cyclone activity in three SRES ensemble experiments with the ECHAM5/MPI-OM1 GCM. *Climate Dynamics*, *29*(2), 195–210. https://doi.org/10.1007/s00382-007-0230-4
Polvani, L. M., Waugh, D. W., Correa, G. J. P., & Son, S.-W. (2011). Stratospheric ozone depletion: The main driver of twentieth-century atmospheric circulation changes in the Southern Hemisphere. *Journal of Climate*, *24*, 795–812.
Schneider, E. K., Kirtman, B. P., & Lindzen, R. S. (1999). Tropospheric water vapor and climate sensitivity. *Journal of the Atmospheric Sciences*, *56*(11), 1649–1658. https://doi.org/10.1175/1520-0469(1999)056<1649:TWVACS>2.0.CO;2
Shaw, T. A., Baldwin, M., Barnes, E. A., Caballero, R., Garfinkel, C. I., Hwang, Y.-T., et al. (2016). Storm track processes and the opposing influences of climate change. *Nature Geoscience*, *9*, 656–664.
Shaw, T. A., & Voigt, A. (2015). Tug of war on summertime circulation between radiative forcing and sea surface warming. *Nature Geoscience*, *8*, 560–566.
Shepherd, T. G. (2014). Atmospheric circulation as a source of uncertainty in climate change projections. *Nature Geoscience*, *7*, 703–708.
Simpson, I. R., Shaw, T. A., & Seager, R. (2014). A diagnosis of the seasonally and longitudinally varying midlatitude circulation response to global warming. *Journal of the Atmospheric Sciences*, *71*, 2489–2515.
Slingo, A., & Slingo, J. M. (1988). The response of a general-circulation model to cloud longwave radiative forcing. Part I: Introduction and initial experiments. *Quarterly Journal of the Royal Meteorological Society*, *114*, 1027–1062. https://doi.org/10.1002/qj.49711448209
Stevens, B., Bony, S., & Webb, M. (2012). Clouds On-Off Klimate Intercomparion Experiment (COOKIE). Retrieved from http://www.euclipse.eu/wp4/wp4.html
Taylor, K. E., Stouffer, R. J., & Meehl, G. A. (2009). A summary of the CMIP5 experiment design. PCMDI Reports. https://pcmdi.llnl.gov/mips/cmip5/experiment_design.html
Taylor, K. E., Stouffer, R. J., & Meehl, G. A. (2012). An overview of CMIP5 and the experiment design. *Bulletin of the American Meteorological Society*, *93*, 485–498.
Tegen, I., Hollrig, P., Chin, M., Fung, I., Jacob, D., & Penner, J. (1997). Contribution of different aerosol species to the global aerosol extinction optical thickness: Estimates from model results. *Journal of Geophysical Research*, *102*(D20), 23,895–23,915.
Thompson, D. W. J., Bony, S., & Li, Y. (2017). Thermodynamic constraint on the depth of the global tropospheric circulation. *PNAS*, *114*(31), 8181–8186.
Ulbrich, U., Leckebusch, G. C., & Pinto, J. G. (2009). Extra-tropical cyclones in the present and future climate: A review. *Theoretical and Applied Climatology*, *96*(1), 117–131.
Ulbrich, U., Pinto, J. G., Kupfer, H., Leckebusch, G. C., Spangehl, T., & Reyers, M. (2008). Changing Northern Hemisphere storm tracks in an ensemble of IPCC climate change simulations. *Journal of Climate*, *21*(8), 1669–1679. https://doi.org/10.1175/2007JCLI1992.1
Vallis, G. K., Zurita-Gotor, P., Cairns, C., & Kidston, J. (2015). Response of the large-scale structure of the atmosphere to global warming. *Quarterly Journal of the Royal Meteorological Society*, *141*, 1479–1501.
Vavrus, S. J. (2018). The influence of arctic amplification on mid-latitude weather and climate. *Current Climate Change Reports*, *4*, 238–249.
Voigt, A., Albern, N., & Papavasileiou, G. (2019). The atmospheric pathway of the cloud-radiative impact on the circulation response to global warming: Important and uncertain. *Journal of Climate*, *32*(10), 3051–3067.
Voigt, A., & Shaw, T. A. (2015). Circulation response to warming shaped by radiative changes of clouds and water vapor. *Nature Geoscience*, *8*, 102–106.

Voigt, A., & Shaw, T. A. (2016). Impact of regional atmospheric cloud-radiative changes on shifts of the extratropical jet stream in response to global warming. *Journal of Climate*, *29*(23), 8399–8421.

Wetherald, R. T., & Manabe, S. (1988). Cloud feedback processes in a general circulation model. *Journal of the Atmospheric Sciences*, *45*(8), 1397–1416.

Woollings, T., Gregory, J. M., Pinto, J. G., Reyers, M., & Brayshaw, D. J. (2012). Response of the North Atlantic storm track to climate change shaped by ocean-atmosphere coupling. *Nature Geoscience*, *5*, 313–317.

Yin, J. H. (2005). A consistent poleward shift of the storm tracks in simulations of 21st century climate. *Geophysical Research Letters*, *32*, L18701. https://doi.org/10.1029/2005GL023684

Zängl, G., Reinert, D., Ripodas, P., & Baldauf, M. (2015). The ICON (ICOsahedral Non-hydrostatic) modelling framework of DWD and MPI-M: Description of the non-hydrostatic dynamical core. *Quarterly Journal of the Royal Meteorological Society*, *141*, 563–579.

Zappa, G., Hoskins, B. J., & Shepherd, T. G. (2015). Improving climate change detection through optimal seasonal averaging: The case of the North Atlantic Jet and European precipitation. *Journal of Climate*, *28*(16), 6381–6397.

Zappa, G., Pithan, F., & Shepherd, T. G. (2018). Multimodel evidence for an atmospheric circulation response to Arctic sea ice loss in the CMIP5 future projections. *Geophysical Research Letters*, *45*, 1011–1019. https://doi.org/10.1002/2017GL076096